Journal of Solid State Chemistry 182 (2009) 2468–2474

Contents lists available at ScienceDirect

Journal of Solid State Chemistry

journal homepage: www.elsevier.com/locate/jssc

Structure, crystal chemistry and thermal evolution of the δ-Bi_2O_3-related phase Bi_9ReO_{17}

Neeraj Sharma [a,*], Ray L. Withers [b], Kevin S. Knight [c], Chris D. Ling [a,d]

[a] School of Chemistry, The University of Sydney, Sydney, NSW 2006, Australia
[b] Research School of Chemistry, Australian National University, Canberra, ACT 0200, Australia
[c] ISIS Facility, Science and Technology Facilities Council, Rutherford Appleton Laboratory, Didcot OX11 0QX, UK
[d] Bragg Institute, Australian Nuclear Science and Technology Organisation, PMB 1, Menai, NSW 2234, Australia

ARTICLE INFO

Article history:
Received 2 April 2009
Received in revised form
11 June 2009
Accepted 4 July 2009
Available online 26 July 2009

Keywords:
Bismuth rhenium oxide
Delta-Bi_2O_3
Neutron powder diffraction
Synchrotron X-ray powder diffraction
Phase transition
Rietveld-refinement

ABSTRACT

The thermal evolution and structural properties of fluorite-related δ-Bi_2O_3-type Bi_9ReO_{17} were studied with variable temperature neutron powder diffraction, synchrotron X-ray powder diffraction and electron diffraction. The thermodynamically stable room-temperature crystal structure is monoclinic $P2_1/c$, $a = 9.89917(5)$, $b = 19.70356(10)$, $c = 11.61597(6)$ Å, $\beta = 125.302(2)^\circ$ ($R_p = 3.51\%$, $wR_p = 3.60\%$) and features clusters of ReO_4 tetrahedra embedded in a distorted Bi–O fluorite-like network. This phase is stable up to 725 °C whereupon it transforms to a disordered δ-Bi_2O_3-like phase, which was modeled with δ-Bi_2O_3 in cubic $Fm\bar{3}m$ with $a = 5.7809(1)$ Å ($R_p = 2.49\%$, $wR_p = 2.44\%$) at 750 °C. Quenching from above 725 °C leads to a different phase, the structure of which has not been solved but appears on the basis of spectroscopic evidence to contain both ReO_4 tetrahedra and ReO_6 octahedra.

1. Introduction

Structures related to the high temperature form of bismuth oxide, δ-Bi_2O_3, generally feature high oxide ion conductivities at temperatures around 750 °C [1,2]. The parent compound δ-Bi_2O_3 has fluorite-type (CaF_2) structure in $Fm\bar{3}m$ symmetry with $a = 5.6595(4)$ Å at 774 °C [3–5]. The oxide ion conduction exhibited by δ-Bi_2O_3 is proposed to be due to the presence of 25% oxygen ion vacancies and the high polarizability of the cation network afforded by Bi^{3+} ions with their $6s^2$ lone pair of electrons [6]. Transition metal dopants, such as Nb^{5+}, Ta^{5+}, Cr^{6+}, Mo^{6+}, W^{6+} and Re^{7+} [7–11] and recently nonmetal dopants such as S^{6+} [12–14] have been used to stabilize δ-Bi_2O_3 to room temperature. These stabilized compounds often have complex modulated structures with δ-Bi_2O_3-type sub-structures and some are known to retain oxide ion conductivities at elevated temperatures similar to that of δ-Bi_2O_3 [2].

Previous studies at the bismuth-rich end of the Bi_2O_3–Re_2O_7 phase diagram have revealed fluorite-related superstructure phases such as $Bi_{28}Re_2O_{49}$ [10,11], containing both tetrahedral ReO_4 and octahedral ReO_6 units, and Bi_3ReO_8 [9], which contains only ReO_4 tetrahedral clusters. Quenched (rapidly cooled from high temperature) phases of composition $Bi_{39}ReO_{62}$, $Bi_{19}ReO_{32}$ and Bi_9ReO_{17} [11] were shown to exhibit both ReO_4 and ReO_6 coordination environments by a combination of diffuse reflectance and Infrared (IR) spectroscopy. The quenched form of Bi_9ReO_{17} was indexed to rhombohedral symmetry with $a = 4.049(4)$ Å and $\alpha = 58.92^\circ$ (or $a = 3.983(4)$ Å, $c = 9.998(8)$ Å in the hexagonal setting), but further structural details were not presented. [11] The structural model for $Bi_{28}Re_2O_{49}$ [10] determined from high resolution neutron diffraction was unable to resolve oxygen atoms bonded to Re sites due to the high levels of orientational disorder associated with these sites. Structurally related compounds such as $Bi_{14}MO_{24}$, M = Cr, W, Mo [15–18] also exhibit this form of orientational disorder. In order to model and/or justify Re coordination environments and fully describe these ordered superstructures, high-resolution diffraction data are required and must be analyzed in conjunction with sound crystal-chemical and charge-balance considerations.

The crystal-chemical considerations in part can be derived from phases with similar compositions (e.g. $Bi_{14}MO_{24}$, M = W, Mo, Cr, S, Re [10,12,15–18]). Similar in composition to Bi_9ReO_{17}, $Bi_8O_{11}(SO_4)$ (= Bi_8SO_{15}) [13] exhibits highly disordered (undefined in refinements) SO_4^{2-} moieties which have been directly related to the high ionic conduction observed at elevated temperatures (i.e. a combination of structural disorder in the O sublattice and rotations of the SO_4 groups). However, two phases are observed in $Bi_8O_{11}(SO_4)$; a room temperature monoclinic phase whose structure could not be solved, and a high temperature phase (above 600 K) indexed in tetragonal $P4_12_12_1$

* Corresponding author. Fax: +61 2 9351 3329.
E-mail address: n.sharma@chem.usyd.edu.au (N. Sharma).

0022-4596/$ - see front matter Crown Copyright © 2009 Published by Elsevier Inc. All rights reserved.
doi:10.1016/j.jssc.2009.07.008

with $a = 11.78840(4)$ and $c = 22.7642(1)$ Å. In $Bi_9SO_{16.5}$, the fluorite-related cell was indexed as tetragonal with parameters $a = 11.024$ and $c = 28.262$ Å but no further structural information or standard deviations on cell parameters was given [14]. These S-containing δ-Bi_2O_3-related phases of similar composition to Bi_9ReO_{17} show complexity and variability involved in both composition and temperature dependence.

This work presents an investigation into the structural properties of the slow-cooled Bi_9ReO_{17} phase using electron, synchrotron X-ray and neutron diffraction techniques. The temperature dependent behavior of Bi_9ReO_{17} is explored to search for possible phase transitions.

2. Experimental

Stoichiometric quantities of Bi_2O_3 (Sigma–Aldrich 5N) and Re metal (Sigma–Aldrich 4N5) were finely ground in an agate mortar and pestle, heated in air at 800 °C for 15 h, and allowed to cool in the furnace to room temperature producing the stable room-temperature phase. A quenched sample was prepared by heating the same sample to 800 °C for 3 h and quenching in air. Initial X-ray powder diffraction (XRD) analysis was carried out on a Shimadzu S6000 XRD using Cu$K\alpha$ radiation. High-resolution XRD data were collected on the Powder Diffraction beamline (10-BM) [19] at the Australian Synchrotron with $\lambda = 0.82667(1)$ Å. IR spectra were collected on a Bruker FT-IR IFS66v spectrometer. Electron diffraction was carried out using a Philips EM 430 transmission electron microscope operating at 300 kV. Samples suitable for TEM work were prepared by the dispersion of finely ground material onto a holey carbon film.

Time-of-flight neutron powder diffraction (NPD) data were collected on the high resolution back-scattering detectors on HRPD at ISIS, Rutherford Appleton Laboratory at room temperature and at 100 °C intervals from 100 to 600 °C then 25 °C intervals from 600 to 825 °C. The sample was sealed in a quartz tube and inserted into a vanadium can. Rietveld-refinements were carried out using the GSAS [20] suite of programs with the EXPGUI [21] front-end.

3. Results

XRD data show differences between the quenched and the slow-cooled samples (Fig. 1). In particular, the slow-cooled sample appears to contain no trace of the quenched sample, and vice versa. For the slow-cooled sample, electron diffraction was used to determine the unit cell, possible space group symmetries and the relationship to the fluorite-type δ-Bi_2O_3 sub-structure. Fig. 2 shows (a) [100], (b) [010] and (c) [001] zone axis electron diffraction patterns (EDPs) of this phase. The fluorite type, sub-structure reflections are labelled with the subscript F while the supercell reflections have no such subscript. The relationship between the two is given by $\mathbf{a}^* = \frac{1}{4}[0\,2\,2]^*_F$, $\mathbf{b}^* = \frac{1}{10}[0\,2\,\bar{2}]^*_F$ and $\mathbf{c}^* = \frac{1}{8}[\bar{2}\,\bar{2}\,4]^*_F$. The corresponding relationship in real space is given by $\mathbf{a} = [111]_F$, $\mathbf{b} = \frac{5}{2}[0\,1\,\bar{1}]_F$ and $\mathbf{c} = [200]_F$. The only observed systematic extinction condition was $F([h0l]^*) = 0$ unless l even (see Fig. 2b) requiring the presence of a c glide perpendicular to **b**. The unit cell was thus found to be monoclinic in either Pc or $P2_1/c$ space group symmetry with cell parameters $a = 9.8990$, $b = 19.7034$, $c = 11.6159$ Å and $\beta = 125.03°$.

The lower symmetry Pc space group was first used in initial efforts to solve the structure. Since this unit cell corresponds to 10 fluorite sub-structure unit cells, it might be expected to contain 40 metal (36 Bi and 4 Re) atoms and 80 oxygen atoms. Direct determination of the metal atom ordering scheme from diffraction data was extremely difficult, as Bi and Re have very similar scattering powers for both X-rays (having 83 and 75 electrons, respectively) and neutrons (with coherent cross-sections of 8.532 and 9.2 fm, respectively). Therefore, as a first step, high-resolution neutron powder diffraction data were used to refine the fluorite-type oxygen site occupancies, exploiting the much greater sensitivity of NPD (compared with XRD) data to oxygen atoms in the presence of heavy metal atoms.

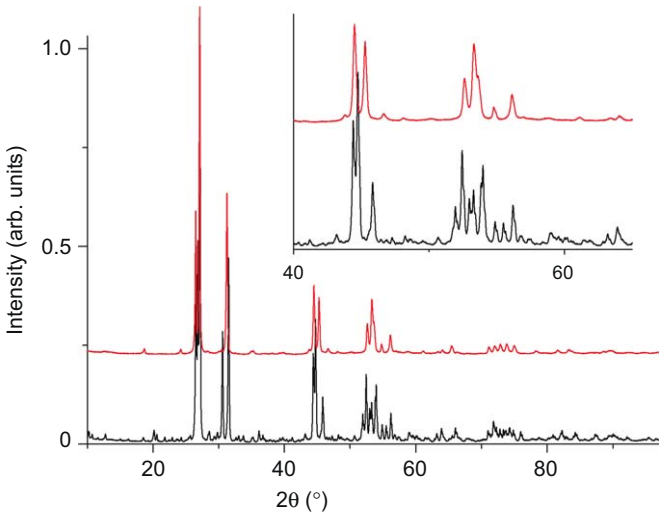

Fig. 1. XRD patterns of the slow-cooled (bottom) and quenched (top) phases of Bi_9ReO_{17}. The inset shows an enlarged section to highlight the differences.

A fluorite-type starting model of stoichiometry BiO_2 was thus constructed in Pc using the subcell–supercell relationship determined using electron diffraction, for Rietveld-refinement against room-temperature NPD data. Oxygen atom site occupancies were then refined. Those that refined to the smallest (or negative) values were then removed, revealing two unique Bi sites whose coordination numbers were reduced from 8 to 4. Identifying these sites as Re is consistent with the required stoichiometry Bi_9ReO_{17} ($Z = 4$). The positions of the oxygen atoms coordinated to the Re atoms were then carefully refined, resulting in the formation of regular ReO_4 tetrahedra. The remaining metal and oxygen atom positions were then allowed to refine (with one Bi site fixed to fluorite-related x and z positions due to the lack of symmetry elements perpendicular to these directions in Pc).

Atomic positions in this refined structure were found to be less than 0.2 Å from obeying the alternative higher symmetry space group $P2_1/c$, which was thus adopted prior to full refinement of cell parameters, atomic positions and independent isotropic atomic displacement parameters (ADPs). This $P2_1/c$ model contains only one unique Re site. The refined cell parameters were $a = 9.89917(5)$, $b = 19.70356(10)$, $c = 11.61597(6)$ Å and $\beta = 125.302(2)°$. Experimental details and refinement statistics are presented in Table 1. The atomic positions, ADPs and calculated bond valence sums (BVS) [22] are presented in Table 2 and selected metal–oxygen bond lengths are presented in Table 3. Final Rietveld-refined room temperature NPD and synchrotron XRD patterns are shown in Fig. 3, the structure in Fig. 4 and the FT-IR spectrum in Fig. 5.

Combined Rietveld-refinements with synchrotron XRD data were subsequently carried out. However, the refined atomic positions and independent ADPs were not significantly changed, nor were their estimated uncertainties significantly improved. We therefore report the results of the refinement against HRPD data alone, in order to avoid the small deterioration in the quality of fit that inevitably arises in combined X-ray and neutron refinements

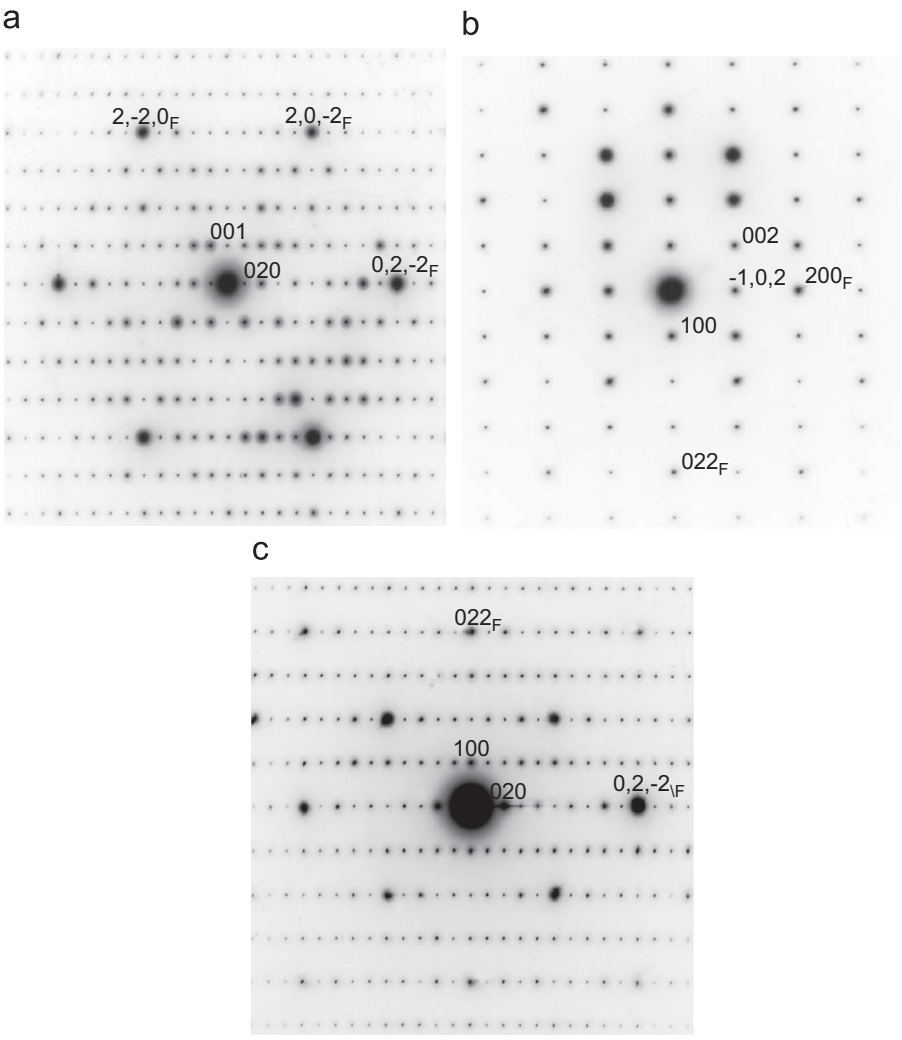

Fig. 2. Zone axis EDPs of slow-cooled Bi_9ReO_{17} (a) [100], (b) [010] and (c) [001]. These correspond to the [111], $\frac{5}{2}[0\,1\,\bar{1}]$ and [200] zone axes of the fluorite-type (F) subcell, respectively.

Table 1
Experimental details.

Composition	Slow-cooled Bi_9ReO_{17}		Bi_9ReO_{17} at 750 °C
Crystal symmetry	Monoclinic		Cubic
Space group	$P2_1/c$		$Fm\bar{3}m$
a (Å)	9.89917 (5)		5.7809 (1)
b (Å)	19.70356 (10)		
c (Å)	11.61597 (6)		
β (deg)	125.302 (2)		
V (Å^3)	1849.05 (2)		193.196 (9)
Radiation	Neutron	Synchrotron	Neutron
Temperature (°C)	20	20	750
Sample quantity (g)	5	0.01	5
Sample environment	Evacuated quartz tube	Sealed quartz capillary	Evacuated quartz tube
Color	Yellow	Yellow	
Data collection	HRPD	10-BM	HRPD
Refinement			
R_p (%)	3.51	1.10	2.49
wR_p (%)	3.60	1.51	2.44
R_F^2 (%)	5.45	8.33	
χ^2 (%)	2.37	1.98	1.7
No. of parameters	130	75	23

Table 2
Final refined fractional atomic coordinates, ADPs and calculated bond valence sums (BVS) for Bi_9ReO_{17} at room temperature.

Atom	Wyckoff position	x	y	z	$U_{iso} \times 100$	BVS
Bi1	8*d*	0.0854 (3)	0.2535 (1)	0.4058 (2)	0.90 (6)	2.82
Bi2	8*d*	0.6095 (3)	0.2730 (1)	0.6861 (2)	1.01 (5)	3.03
Bi3	8*d*	0.1021 (3)	0.0520(1)	0.4369 (2)	1.11 (6)	3.11
Bi4	8*d*	0.1354 (3)	0.4460 (1)	0.4410 (2)	0.79 (5)	3.25
Bi5	8*d*	0.6223 (3)	0.4523 (1)	0.6769 (2)	1.14 (6)	2.92
Bi6	8*d*	0.0849 (3)	0.6467 (1)	0.3926 (2)	1.12 (6)	3.09
Bi7	8*d*	0.1120 (3)	0.8445 (1)	0.4476 (2)	0.60 (6)	3.24
Bi8	8*d*	0.6589 (3)	0.8440 (1)	0.1936 (2)	0.97 (6)	2.96
Bi9	8*d*	0.6243 (3)	0.6659 (1)	0.1885 (2)	0.97 (6)	3.18
Re1	8*d*	0.6330 (3)	0.4383 (1)	0.1807 (2)	1.28 (6)	7.57
O1	8*d*	0.4545 (6)	0.1068 (2)	0.6252 (5)	3.77 (11)	1.94
O2	8*d*	0.6435 (4)	0.4550 (2)	0.0367 (3)	2.10 (9)	1.74
O3	8*d*	0.3545 (6)	0.4856 (2)	0.7423 (6)	4.77 (13)	2.10
O4	8*d*	0.1972 (6)	0.8904 (2)	0.1966 (5)	3.56 (12)	2.05
O5	8*d*	0.4474 (4)	0.2433 (2)	0.7588 (4)	1.58 (8)	2.15
O6	8*d*	0.9083 (4)	0.2496 (2)	0.1702 (4)	1.42 (10)	2.13
O7	8*d*	0.5218 (5)	0.3637 (2)	0.7231 (4)	2.41 (10)	2.20
O8	8*d*	0.6737 (5)	0.1336 (2)	0.0977 (4)	1.81 (10)	1.91
O9	8*d*	0.3137 (4)	0.2422 (2)	0.8979 (4)	0.69 (8)	2.17
O10	8*d*	0.8308 (4)	0.2727 (2)	0.8922 (4)	1.28 (8)	2.18
O11	8*d*	0.8892 (4)	0.4367 (2)	0.9277 (4)	1.29 (8)	2.07
O12	8*d*	0.3671 (4)	0.0344 (2)	0.9793 (4)	1.53 (8)	2.00
O13	8*d*	0.0805 (5)	0.3535 (2)	0.8282 (4)	1.45 (9)	2.36
O14	8*d*	0.1544 (4)	0.1582 (2)	0.1181 (4)	1.46 (8)	2.00
O15	8*d*	0.1061 (4)	0.1303 (2)	0.8093 (4)	1.05 (9)	2.14
O16	8*d*	0.1284 (4)	0.3347 (2)	0.0936 (4)	1.06 (8)	2.15
O17	8*d*	0.0372 (6)	0.9752 (2)	0.7802 (5)	3.29 (11)	1.93

Full details, including bond lengths and angles, are available in the deposited crystallographic information file (CIF).

Table 3
Selected metal–oxygen bond lengths (Å) in the refined structure of Bi_9ReO_{17}.

Bi1–O6	2.24 (1)	Bi6–O13	2.1 (1)
Bi1–O13	2.28 (1)	Bi6–O6	2.17 (1)
Bi1–O9	2.31 (1)	Bi6–O14	2.31 (1)
Bi1–O10	2.48 (1)	Bi6–O8	2.34 (1)
Bi1–O15	2.60 (1)	Bi6–O17	2.64 (1)
Bi1–O16	2.62 (1)	Bi6–O4	3.12 (1)*
Bi1–O14	2.76 (1)	Bi6–O10	3.27 (1)
Bi1–O4	3.56 (1)*	Bi7–O10	2.13 (1)
Bi2–O10	2.11 (1)	Bi7–O16	2.14 (1)
Bi2–O7	2.13 (1)	Bi7–O6	2.25 (1)
Bi2–O5	2.28 (1)	Bi7–O11	2.32 (1)
Bi2–O8	2.36 (1)	Bi7–O15	2.52 (1)
Bi2–O9	2.92 (1)	Bi7–O2	3.18 (1)*
Bi2–O6	3.10 (1)	Bi7–O7	3.45 (1)
Bi2–O1	3.51 (1)*	Bi7–O4	3.59 (1)*
Bi2–O4	3.59 (1)*	Bi8–O9	2.10 (1)
Bi3–O11	2.06 (1)	Bi8–O16	2.13 (1)
Bi3–O17	2.13 (1)	Bi8–O5	2.24 (1)
Bi3–O13	2.18 (1)	Bi8–O15	2.39 (1)
Bi3–O11	2.74 (1)	Bi8–O12	3.04 (1)
Bi3–O16	2.79 (1)	Bi8–O1	3.06 (1)*
Bi3–O2	3.03 (1)*	Bi8–O8	3.10 (1)
Bi3–O1	3.05 (1)*	Bi9–O14	2.04 (1)
Bi4–O15	2.04 (1)	Bi9–O5	2.13 (1)
Bi4–O12	2.10 (1)	Bi9–O7	2.28 (1)
Bi4–O17	2.17 (1)	Bi9–O9	2.31 (1)
Bi4–O14	2.84 (1)	Bi9–O13	3.06 (1)
Bi4–O4	2.92 (1)*	Bi9–O3	3.07 (1)*
Bi4–O3	2.96 (1)*	Bi9–O2	3.40 (1)*
Bi4–O7	3.68 (1)	Bi9–O1	3.46 (1)*
Bi5–O8	2.12 (1)	Re1–O1	1.73 (1)*
Bi5–O7	2.22 (1)	Re1–O2	1.76 (1)*
Bi5–O12	2.24 (1)	Re1–O3	1.71 (1)*
Bi5–O12	2.47 (1)	Re1–O4	1.72 (1)*
Bi5–O11	2.58 (1)		
Bi5–O17	3.14 (1)		
Bi5–O3	3.22 (1)*		

The bonds where the O site is involved with ReO_4 is marked with *.

due to different absorption, extinction, preferred orientation, etc. parameters. Rietveld-refinement against synchrotron XRD data was nevertheless undertaken as an independent check on the final model refined against HRPD data, using a minimal set of variables (peak shape, background, instrumental parameters and global isotropic ADPs for each atomic species). The quality of the fit obtained provides a strong validation of that model (Fig. 3b).

Fig. 6 shows a Rietveld fit to NPD data collected at 750 °C, modeled as a disordered δ-Bi_2O_3-like phase [4] in cubic $Fm\bar{3}m$ space group symmetry with cell parameter $a = 5.7809(1)$ Å.

From variable temperature NPD data, the variation in unit cell parameters as a function of temperature was also determined as shown in Fig. 7a. All cell lengths show a near-linear increase with temperature, although the relative growth of the *b*-axis (2.1%) is ~3 times greater than the *a* and *c* axes (1.2% and 1.2 %, respectively). Cell volume (Fig. 7b) increases linearly with temperature until the transition into the disordered δ-Bi_2O_3-like high temperature structure, where a discontinuity is observed.

For refinements against variable temperature NPD data, oxygen atoms coordinated exclusively to Bi (i.e. in the fluorite-like part of the structure, hereafter referred to as O_{Bi}) were assigned one global isotropic ADP, and oxygen atoms coordinated to Re in ReO_4 tetrahedra (hereafter referred to as O_{Re}) were assigned another global isotropic ADP. Fig. 8 shows that the ADPs of O_{Re} increase faster with temperature than those of O_{Bi}. Fig. 8 also shows increasing average Re–O bond length with temperature.

4. Discussion

The slow-cooled phase of Bi_9ReO_{17} shows a number of features consistent with other reported Bi–Re^{7+}–O phases such as $Bi_{28}Re_2O_{49}$ [10] and Bi_3ReO_8. [9] Re–O bonds are less than or equal to 1.765(4) Å, and of those O sites bonded to Re, none are closer than 2.919(5) Å to a Bi site. The assignment of the metal cation array is confirmed with all Bi–O bonds greater than 2.044(4) Å and metal ADPs below 0.012(1) $Å^2$. ReO_4 tetrahedra are near-ideal with O–Re–O angles between 107° and 113° and Re–O bonds between 1.711(6) and 1.765(4) Å using a completely unconstrained refinement of atomic positions, illustrating the coordination of Re is valid. Calculated BVS (Table 2) show no large discrepancies from nominal valencies (Bi^{3+}, Re^{7+} and O^{2-}). The fluorite-like nature of the Bi-rich part of the ambient temperature Bi_9ReO_{17} phase is preserved and seems to "bend" around the clustered ReO_4 units when viewed along $[100] = \langle 111 \rangle_F$ (Fig. 4). Bi1, Bi2, Bi7 and Bi9 have 8-fold coordination polyhedra that can be directly related to ideal fluorite-type, while Bi3, Bi4, Bi5, Bi6 and Bi8 are 7-fold coordinate (i.e. they have one oxygen vacancy associated with them with respect to ideal fluorite-type). In all cases, however, they are highly distorted due to the short Re–O bonds required to satisfy the bonding requirements of Re^{7+} in tetrahedral coordination.

Unit cell axes and volume follow near-linear trends with increasing temperature, a result of thermal expansion. The long *b*-axis grows much more rapidly than the *c* and *a* axes (Fig. 7), although the reason for this is not clear. Increases in O_{Re} ADPs indicate significant thermal motion around the Re site. The only observed anomaly with increasing temperature was an 8.0% increase in the average Re–O bond lengths, which is ~4 times greater than the expansion of the unit cell. This corresponds to the sample adopting an average δ-Bi_2O_3-type structure at high temperature. O's bonded to Re are furthest away from the average fluorite-type positions in the slow-cooled phase, and therefore are expected to displace to a greater extent than O's part of the Bi–O network as temperature increases.

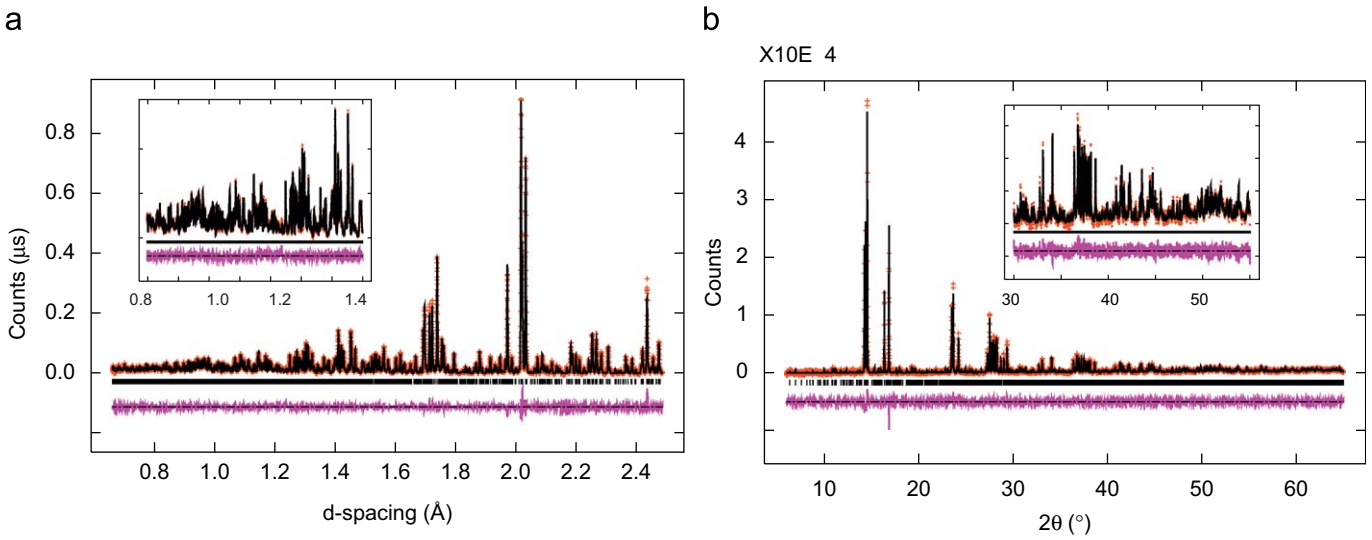

Fig. 3. Final fit to Rietveld-refined (a) NPD and (b) synchrotron XRD data for ambient temperature Bi_9ReO_{17}. Observed data are shown as crosses (+), calculated data as solid lines, the difference as a solid line below and Bragg peak markers as vertical lines below. Overall powder *R*-factors for NPD: $R_p = 3.51\%$, $wR_p = 3.60\%$, $R_F^2 = 5.45\%$ and $\chi^2 = 2.37$ for 130 refined parameters. Overall powder *R*-factors for synchrotron XRD: $R_p = 1.10\%$, $wR_p = 1.51\%$, $R_F^2 = 8.33\%$ and $\chi^2 = 1.98$ for 75 refined parameters.

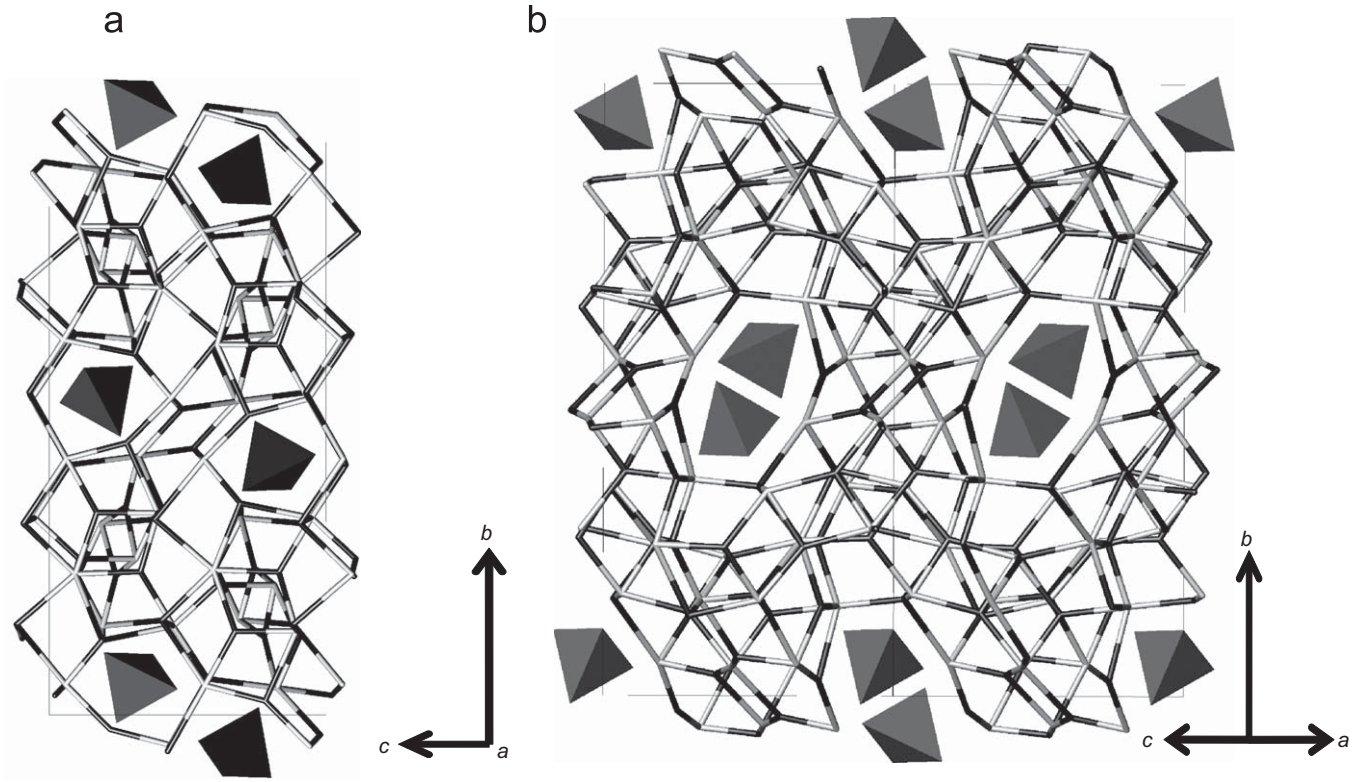

Fig. 4. The crystal structure of Bi_9ReO_{17} viewed along the (a) [100] and (b) [101] directions. Bi atoms and bonds are light gray, O atoms and bonds are black and ReO_4 are represented by gray tetrahedra.

From the high temperature disordered δ-Bi_2O_3-type phase, slow-cooling can result in the tetrahedral Re environments described in this model or quenching can result in the dual Re coordination environments in light of the work of Fries et al. [11] and Re bonding environments of $Bi_{28}Re_2O_{49}$ [10]. Fries et al. [11] present the case for 6-fold coordination around Re in quenched Bi_9ReO_{17} on the basis of a small feature in the FT-IR spectrum which was slightly shifted relative to a reference sample. Our results clearly show that the coordination environment of Re in the slow-cooled phase is entirely tetrahedral. Fig. 5 shows the FT-IR spectrum of our slow-cooled sample, which also shows a feature around 900 cm^{-1} in good agreement with the one assigned to tetrahedral Re in Bi_3ReO_8 [9].

Fries et al. [11] also use color (measured by diffuse reflectance) as an indicator of Re environments and distribution. As *x* is increased in the formulation $Bi_{2-x}Re_xO_{3+2x}$, the color changes from deep orange to yellow-orange, with Bi_3ReO_8 (containing only ReO_4 units) being pale yellow. The yellow coloring signifies the

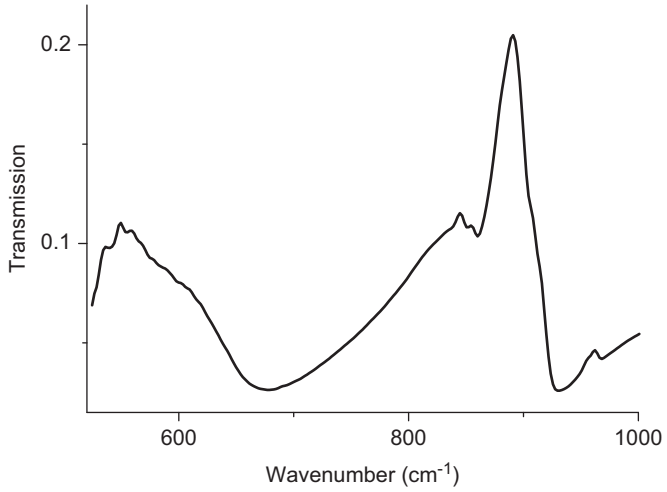

Fig. 5. FTIR spectrum of Bi_9ReO_{17}.

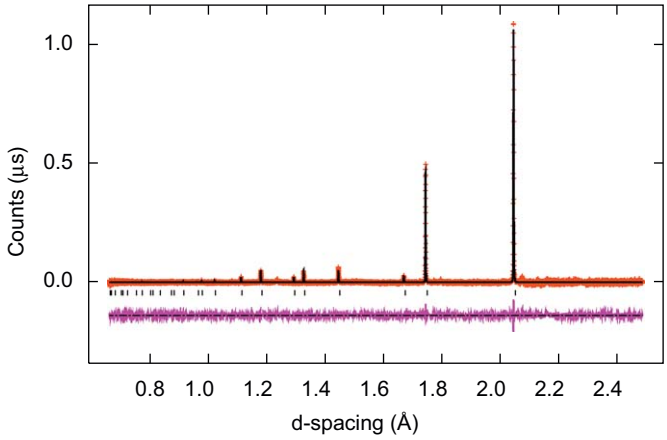

Fig. 6. Final Rietveld fit to NPD data at 750 °C for Bi_9ReO_{17} modeled as δ-Bi_2O_3 in cubic $Fm\bar{3}m$ symmetry [4] with $a = 5.7809(1)$ Å at 750 °C. Observed data are shown as crosses (+), calculated data as solid lines, the difference as a solid line below and Bragg peak markers as vertical lines below. Overall powder *R*-factors for NPD: $R_p = 2.49\%$, $wR_p = 2.44\%$ and $\chi^2 = 1.7$ for 23 refined parameters. The weak additional peaks at $d \sim 1.25$ and 2.5 Å are due to the quartz tube in which the sample was sealed.

transition of the compound from β-Bi_2O_3-related to δ-Bi_2O_3-related sub-structures. The quenched Bi_9ReO_{17} sample is a yellow-orange color, while the slow-cooled Bi_9ReO_{17} sample is a pale-yellow color similar to the yellow-colored Bi_3ReO_8 reinforcing the presence of only ReO_4 units. The quenched sample may contain both tetrahedral and octahedral Re bonding environments as the color is similar to the Re-rich samples which are known to exhibit both coordination environments. This contributes to the ongoing difficulties in solving the structure of the quenched form.

Probably the most similar compounds to Bi_9ReO_{17} in the literature are $Bi_8O_{11}(SO_4)$ [13] and $Bi_9SO_{16.5}$ [14] both of which have been indexed to tetragonal cells. At these compositions in S- and Re-containing δ-Bi_2O_3-related structures, pairing of ReO_4/SO_4 tetrahedra are observed. The slow-cooled phase of $Bi_8O_{11}(SO_4)$ was termed the "complex monoclinic phase" and not solved, but transformed at 600 K to the slightly disordered tetragonal phase. No such transformation was observed in Bi_9ReO_{17}. Bi_9ReO_{17} therefore appears to have more ordered tetrahedra than $Bi_8O_{11}(SO_4)$. This implies that the oxide ion conduction properties of Bi_9ReO_{17} should be inferior to those of $Bi_8O_{11}(SO_4)$ at lower temperatures.

Crumpton et al. [15] found for $Bi_{14}MO_{24}$, M = Mo, Cr, W that lowering the temperature close to or below room temperature induces a phase transition from the orientationally disordered MO_4 moieties in tetragonal $I4/m$ symmetry to slightly more ordered MO_4 in monoclinic $C2/m$, a transition also noted for the M = S analog [12]. The existence of low and high temperature phases at this composition and in $Bi_8O_{11}(SO_4)$ [13] led to the expectation of an orientationally disordered form of the room-temperature Bi_9ReO_{17} phase at intermediate temperatures. However, our variable temperature NPD data contained no evidence for such a phase prior to complete disordering into a δ-Bi_2O_3-like high temperature phase.

5. Conclusions

The slow-cooled room temperature phase of Bi_9ReO_{17} is an ordered δ-Bi_2O_3-type superstructure with monoclinic $P2_1/c$ space-group symmetry, $a = 9.89917(5)$, $b = 19.70356(10)$, $c = 11.61597(6)$ Å and $\beta = 125.302(2)^\circ$. It features clusters of ReO_4 tetrahedra embedded in a fluorite-type Bi–O network which slightly distorts to "bend" around the ReO_4 clusters. On heating, the ReO_4 become

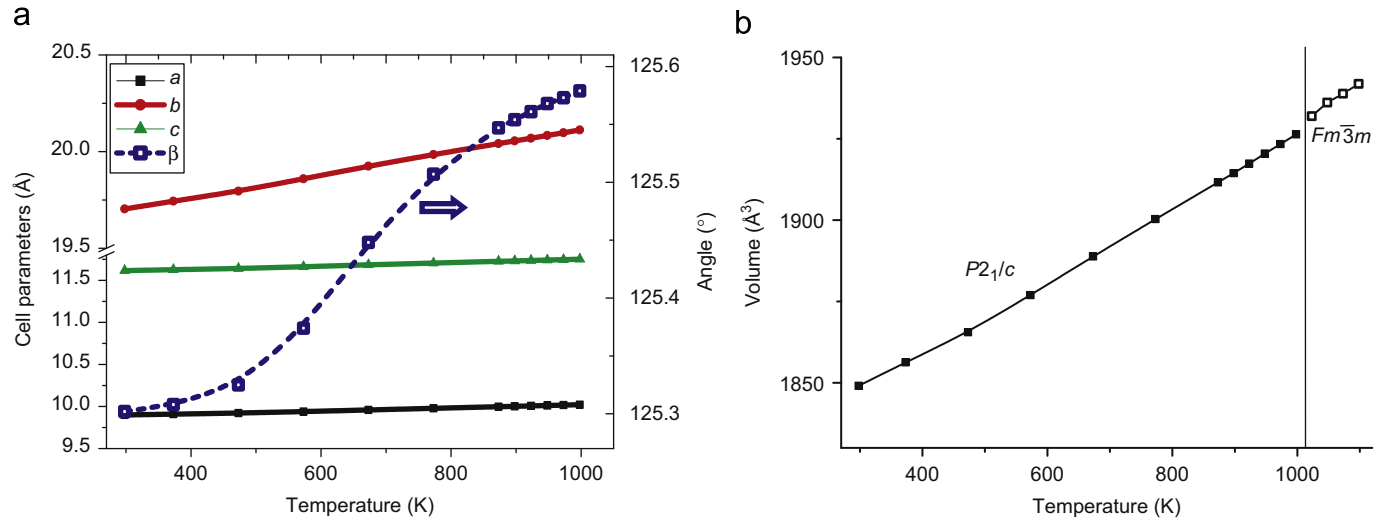

Fig. 7. (a) Unit cell parameters as a function of temperature below the transition into the high temperature phase. (b) Unit cell volume as a function of temperature with the high temperature phase represented by a 10 × supercell of δ-Bi_2O_3.

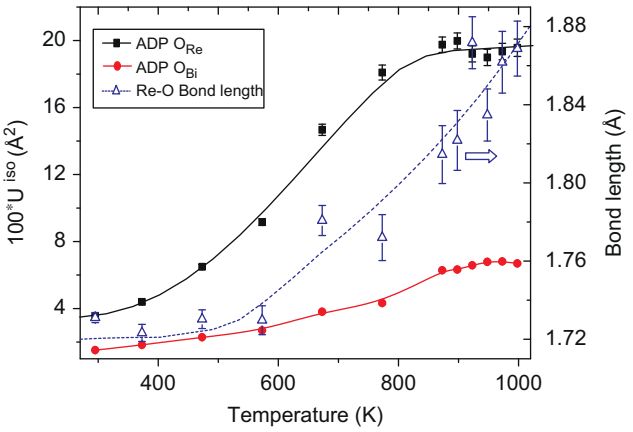

Fig. 8. Thermal dependence of constrained ADPs for oxygen atoms not bonded to Bi (O_{Bi}, red circles) and those bonded to Re (O_{Re}, black squares). Average Re–O bond lengths are shown as open blue triangles (right-hand side axis). Lines are guides to the eye.

disordered at a faster rate than the rest of the structure, and expand at a faster rate than the unit cell. Above 725 °C, the compound transforms to the average cubic δ-Bi_2O_3-type structure, accompanied by a slight volume expansion. Quenching from above 725 °C leads to a different phase, the structure of which has not been solved but which appears on the basis of spectroscopic evidence to contain both ReO_4 tetrahedra and ReO_6 octahedra.

Acknowledgments

This work was supported by the Australian Research Council (ARC)—Discovery Projects (DP0666465 and DP0877695) and the Australian Institute of Nuclear Science and Engineering Postgraduate Research Awards scheme. Experiments at the ISIS Pulsed Neutron and Muon Source were supported by a beamtime allocation from the Science and Technology Facilities Council and the ARC LIEF Grant "Access for Australian Researchers to Advanced Neutron Beam Techniques". We would like to thank Prof. B.J. Kennedy, Dr. Q. Zhou and Mr. J. Ting for collecting synchrotron diffraction patterns.

References

[1] N.M. Sammes, G.A. Tompsett, H. Nafe, F. Aldinger, J. Eur. Ceram. Soc. 19 (1999) 1801–1826.
[2] T. Takahashi, H. Iwahara, Mater. Res. Bull. 13 (1978) 1447–1453.
[3] G. Gattow, H. Schröder, Z. Anorg. Allg. Chem. 318 (1962) 176–189.
[4] P.D. Battle, C.R.A. Catlow, J. Drennan, A.D. Murray, J. Phys. C: Solid State Phys. 16 (1983) L561–L566.
[5] H.A. Harwig, Z. Anorg. Allg. Chem. 444 (1978) 151–166.
[6] J.C. Boivin, G. Mairesse, Chem. Mater. 10 (1998) 2870–2888.
[7] C.D. Ling, R.L. Withers, S. Schmid, J.G. Thompson, J. Solid State Chem. 137 (1998) 42–61.
[8] Y.H. Liu, J.B. Li, J.K. Liang, J. Luo, L.N. Ji, J.Y. Zhang, G.H. Rao, Mater. Chem. Phys. 112 (2008) 239–243.
[9] A.K. Cheetham, A.R.R. Smith, Acta Crystallogr. B 41 (1985) 225–230.
[10] T.E. Crumpton, J.F.W. Mosselmans, C. Greaves, J. Mater. Chem. 15 (2005) 164–167.
[11] T. Fries, G. Lang, S. Kemmler-Sack, Solid State Ionics 89 (1996) 233–240.
[12] M.G. Francesconi, A.L. Kirbyshire, C. Greaves, O. Richard, G. Van Tendeloo, Chem. Mater. 10 (1998) 626–632.
[13] T.E. Crumpton, C. Greaves, J. Mater. Chem. 14 (2004) 2433–2437.
[14] V.I. Smirnov, V.G. Ponomareva, Yu.M. Yukhin, N.F. Uvarov, Solid State Ionics 156 (2003) 79–84.
[15] T.E. Crumpton, M.G. Francesconi, C. Greaves, J. Solid State Chem. 175 (2003) 197–206.
[16] C.D. Ling, Physica B 385–386 (2006) 193–195.
[17] C.D. Ling, R.L. Withers, J.G. Thompson, S. Schmid, Acta Crystallogr. B 55 (1999) 306–312.
[18] G. Spinolo, C. Tomasi, Powder Diffr. 12 (1997) 16–19.
[19] K.S. Wallwork, B.J. Kennedy, D. Wang, in: AIP Conference Proceedings, 2007, p. 879.
[20] A.C. Larson, R.B. Von Dreele, General structure analysis system (GSAS), Los Alamos National Laboratory Report LAUR 86-748, 1994.
[21] B.H. Toby, EXPGUI, a graphical user interface for GSAS, 2001.
[22] N.E. Brese, M. O'Keeffe, Acta Crystallogr. B 47 (1991) 192–197.